

Enzymatic Regulation of Protein-Protein Interactions in Artificial Cells

Citation for published version (APA):

van Veldhuisen, T. W., Altenburg, W. J., Verwiel, M. A. M., Lemmens, L. J. M., Mason, A. F., Merks, M., Brunsveld, L., & van Hest, J. C. M. (2023). Enzymatic Regulation of Protein-Protein Interactions in Artificial Cells. *Advanced Materials*, 35(29), Article 2300947. <https://doi.org/10.1002/adma.202300947>

Document license:
CC BY-NC

DOI:
[10.1002/adma.202300947](https://doi.org/10.1002/adma.202300947)

Document status and date:
Published: 20/07/2023

Document Version:
Publisher's PDF, also known as Version of Record (includes final page, issue and volume numbers)

Please check the document version of this publication:

- A submitted manuscript is the version of the article upon submission and before peer-review. There can be important differences between the submitted version and the official published version of record. People interested in the research are advised to contact the author for the final version of the publication, or visit the DOI to the publisher's website.
- The final author version and the galley proof are versions of the publication after peer review.
- The final published version features the final layout of the paper including the volume, issue and page numbers.

[Link to publication](#)

General rights

Copyright and moral rights for the publications made accessible in the public portal are retained by the authors and/or other copyright owners and it is a condition of accessing publications that users recognise and abide by the legal requirements associated with these rights.

- Users may download and print one copy of any publication from the public portal for the purpose of private study or research.
- You may not further distribute the material or use it for any profit-making activity or commercial gain
- You may freely distribute the URL identifying the publication in the public portal.

If the publication is distributed under the terms of Article 25fa of the Dutch Copyright Act, indicated by the "Taverne" license above, please follow below link for the End User Agreement:

www.tue.nl/taverne

Take down policy

If you believe that this document breaches copyright please contact us at:

openaccess@tue.nl

providing details and we will investigate your claim.

Enzymatic Regulation of Protein–Protein Interactions in Artificial Cells

Thijs W. van Veldhuisen, Wiggert J. Altenburg, Madelief A. M. Verwiel, Lenne J. M. Lemmens, Alexander F. Mason, Maarten Merkx, Luc Brunsveld,* and Jan C. M. van Hest*

Membraneless organelles are important for spatial organization of proteins and regulation of intracellular processes. Proteins can be recruited to these condensates by specific protein–protein or protein–nucleic acid interactions, which are often regulated by post-translational modifications. However, the mechanisms behind these dynamic, affinity-based protein recruitment events are not well understood. Here, a coacervate system that incorporates the 14-3-3 scaffold protein to study enzymatically regulated recruitment of 14-3-3-binding proteins is presented, which mostly bind in a phosphorylation-dependent manner. Synthetic coacervates are efficiently loaded with 14-3-3, and phosphorylated binding partners, such as the c-Raf pS233/pS259 peptide (c-Raf), show 14-3-3-dependent sequestration with up to 161-fold increase in local concentration. The c-Raf domain is fused to green fluorescent protein (GFP-c-Raf) to demonstrate recruitment of proteins. In situ phosphorylation of GFP-c-Raf by a kinase leads to enzymatically regulated uptake. The introduction of a phosphatase into coacervates preloaded with the phosphorylated 14-3-3-GFP-c-Raf complex results in a significant cargo efflux mediated by dephosphorylation. Finally, the general applicability of this platform to study protein–protein interactions is demonstrated by the phosphorylation-dependent and 14-3-3-mediated active reconstitution of a split-luciferase inside artificial cells. This work presents an approach to study dynamically regulated protein recruitment in condensates, using native interaction domains.


1. Introduction

Spatial organization of intracellular proteins is essential for the coordination of the many distinct processes carried out inside the cell. Cells have several ways to regulate protein activity, for example by placing interaction partners in close proximity inside an organelle or at the plasma membrane.^[1,2] Alternatively, interacting proteins can also be (co-)assembled into supramolecular complexes by so-called scaffold proteins.^[1,3] Scaffold proteins are key regulators of cellular signaling by spatially coordinating proteins that are involved in signaling pathways, leading to signal enhancement, allosteric effects, or tethering of multiple proteins.^[1,4] These scaffold proteins generally have multiple binding sites to allow for multivalent interactions with a single target protein or binding to two or more different target proteins, thereby activating or deactivating certain signaling pathways.^[1] The protein–protein interactions (PPIs) established on scaffold proteins are often regulated by post-translational modifications such as phosphorylation.^[1,3]

Biomolecular condensates are intracellular liquid–liquid phase separated (LLPS) droplets comprised of proteins and/or nucleic acids and are another example

of a dedicated molecular environment for organization and dynamic recruitment of proteins.^[5–8] Such droplets have been shown to be essential to intracellular organization of proteins and signaling networks.^[9–11] The recruitment into condensates of client proteins, which are proteins that are non-essential to condensate formation, is typically governed by protein–protein or protein–nucleic acid interactions, involving disordered protein domains or programmed interaction motifs such as folded protein domains.^[5,6,10,12–14] Client proteins can have their function altered by recruitment to condensates; kinases are for example known to change their activity and expand their substrate specificity when inside condensates, leading to the phosphorylation of non-canonical substrates and alteration in signaling pathways.^[15] Hence, condensates can serve as a regulatory hub for PPIs; the protein network found in stress granules,^[16,17] which are membraneless organelles that respond to stress by promoting cell

T. W. van Veldhuisen, W. J. Altenburg, M. A. M. Verwiel, L. J. M. Lemmens, A. F. Mason, M. Merkx, L. Brunsveld, J. C. M. van Hest
Laboratory of Chemical Biology
Department of Biomedical Engineering
and Institute for Complex Molecular Systems
Eindhoven University of Technology
P.O. Box 513, MB Eindhoven 5600, The Netherlands
E-mail: l.brunsveld@tue.nl; j.c.m.v.hest@tue.nl

 The ORCID identification number(s) for the author(s) of this article can be found under <https://doi.org/10.1002/adma.202300947>

© 2023 The Authors. Advanced Materials published by Wiley-VCH GmbH. This is an open access article under the terms of the Creative Commons Attribution-NonCommercial License, which permits use, distribution and reproduction in any medium, provided the original work is properly cited and is not used for commercial purposes.

DOI: 10.1002/adma.202300947

survival, was found to consist of a diverse proteome of more than 200 proteins.^[16] The protein composition of stress granules is dynamic and stress-dependent, where PPIs are thought to regulate translational responses to stress.^[16,17] These PPIs can be enzymatically regulated by kinase recruitment to the stress granule, which influences the assembly and activity of the stress granule.^[18] Altered stress granule dynamics and composition have been found in for example amyotrophic lateral sclerosis patients, linking condensates to neurodegenerative diseases.^[16] Furthermore, condensates were found to be able to accelerate or decelerate the aggregation of the amyloidogenic protein α -synuclein.^[19]

Despite their importance, our understanding of the dynamic and often short-lived PPIs that play a role in recruitment to condensates is limited, partly because of the complexity of the living cell, which makes a focused investigation of the recruitment and organizational process challenging. Recent advances in the field of artificial cell platforms offer well-defined systems that can mimic the intracellular milieu.^[20] Unlike other artificial cells or organelles such as giant unilamellar vesicles and polymersomes, synthetic LLPS droplets or coacervates are well suited for this purpose, as they display a crowded interior that closely resembles the dense molecular environment of the cytoplasm and membraneless organelles.^[20,21] Engineered droplets reconstituted by recombinant proteins in solution^[15,22–25] or expressed in cells^[23,24,26–28] have been applied to study biophysical phenomena or to regulate cellular functions by recruitment of cargo proteins. The assembly of such phase-separated droplets can be based on specific PPIs such as rapamycin-induced interactions,^[15,25,27] coiled-coil peptide interactions,^[24] or SH3 domain interactions.^[29] Cells feature many membraneless organelles that can coexist with metastable properties, unlike engineered condensates which undergo Ostwald ripening and fusion unless stabilized.^[21] Stabilized droplets based on synthetic polyelectrolytes and a membrane-forming triblock copolymer have previously been reported by us,^[30–32] and this system was applied to specifically recruit protein cargo mediated by interactions between His-tags and polyelectrolyte moieties,^[32] with a coacervate stability of several days.^[33]

Synthetic protein affinity pairs have been used for the recruitment of client proteins such as fluorescent proteins^[24,29] and enzymes^[15,25] to synthetic condensates in vitro, and of native cytosolic proteins to synthetic condensates inside cells.^[27] However, the recruitment of client proteins using native interaction domains has not been studied extensively in engineered condensates. Such synthetic systems present a unique platform in which biologically relevant dynamic interactions could be studied in a controlled manner.

One of the most important scaffold proteins found in the cell is the dimeric 14-3-3 protein with a large interactome of more than 500 proteins,^[34] such as the RAF kinases,^[35,36] which are involved in cell proliferation, and the tumor suppressor protein p53.^[37,38] Most of the 14-3-3 interaction partners bind in a phosphorylation-dependent manner,^[39] although there are also interaction partners with a phosphorylation-independent binding mode.^[40] Furthermore, selected 14-3-3 PPIs can also be stabilized with small molecules, making this also a pharmaceutically relevant target class.^[41] 14-3-3 has also been used as a model protein for bottom-up synthetic signaling systems, employing programmable interactions with its interaction partners.^[42,43]

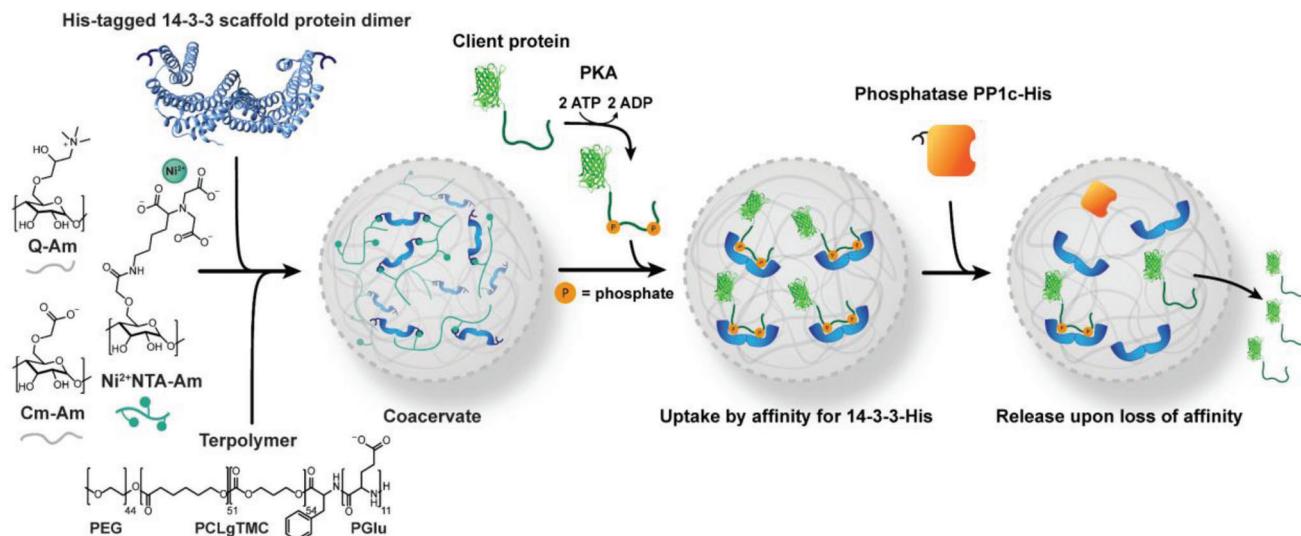
In this work, we present a coacervate platform, based on associative liquid–liquid phase separation, which incorporates the 14-3-3 scaffold protein to evaluate affinity-based and enzymatically-regulated recruitment and binding of its interaction partners within the dense condensate environment (**Scheme 1**). The synthetic condensate is composed of positively charged quaternized amylose (Q-Am) and negatively charged carboxymethylated amylose (Cm-Am), with an overall excess of positive charge.^[30,32] By incorporating nitrilo triacetic acid modified amylose complexed with Ni^{2+} (Ni-NTA-Am), His-tagged protein cargo can be embedded in a programmed manner based on its affinity for Ni-NTA-Am.^[32] By anchoring His-tagged 14-3-3 (14-3-3-His) inside the coacervates, non-His-tagged 14-3-3 binding partners (client proteins) can be localized in the droplets. The coacervates are stabilized with a semipermeable triblock copolymer membrane,^[30] yielding an artificial cell with a stability that allows us to study the recruitment of client proteins and regulation of PPIs. Because the affinity of the client proteins for 14-3-3 is dependent on their phosphorylation state, uptake and release can be controlled by the action of a kinase and phosphatase, respectively. The system presented here demonstrates that artificial cell platforms can be explored to mimic naturally occurring intracellular protein recruitment processes in a highly controlled environment.

2. Results and Discussion

2.1. Affinity-Based Uptake of 14-3-3 Client Peptides in Coacervates

Coacervates were prepared in a 3:0.8:0.2 charge ratio of Q-Am/Cm-Am/NTA-Am, which was found to give the most stable coacervates with efficient uptake of His-tagged proteins. The terpolymer membrane that coats the coacervate interface is dynamic, disordered, and semipermeable to macromolecular cargo such as proteins.^[31,32] Fluorescently labeled 14-3-3-His was sequestered in the coacervates, with a median local concentration of $64 \pm 15 \mu\text{M}$ across three independent samples, as calculated using a calibration curve of fluorescence intensity (Figures S1 and S2, Supporting Information). This represents a 640-fold locally enhanced concentration compared to a bulk concentration of 100 nM. To evaluate the capacity of this platform for recruitment, first several fluorescein isothiocyanate (FITC)-labeled peptide derivatives of 14-3-3 binding partners were selected for evaluation of their 14-3-3-dependent uptake in coacervates. These binding partners, reflecting a diversity of physicochemical properties, 14-3-3 affinity, and 14-3-3 binding modes,^[44] are shown in **Table 1**. The peptides ChREBP and BiExoS were added to represent phosphorylation-independent clients; the ChREBP $\alpha 2$ helix is known to bind to 14-3-3 mediated by electrostatic as well as van der Waals interactions.^[45] The BiExoS peptide was derived from Exoenzyme S, which has a 14-3-3 binding motif with Asp residues that interact with 14-3-3 in a similar manner as phosphorylated residues.^[46] The non-phosphorylated c-Raf S233/S259 peptide was added as a non-binding, negative control. Fluorescence anisotropy (FA) assays in bulk were used to determine the affinity of the peptides for 14-3-3 (Figure S3, Supporting Information).

The coacervates can sequester cargo based on its physicochemical properties; negatively charged macromolecules will



Scheme 1. Schematic overview of coacervate preparation and affinity-based, enzymatically regulated uptake of 14-3-3 binding partners. Positively charged Q-Am and negatively charged Cm-Am and Ni-NTA-Am are mixed to form coacervates. His-tagged 14-3-3 (14-3-3-His) is loaded and the terpolymer is added to stabilize the coacervates with a semipermeable membrane. 14-3-3 binding partners (client proteins) can be taken up based on their affinity for 14-3-3-His, which can be regulated by their phosphorylation state. In situ phosphorylation of binding partners by a kinase leads to an increase in affinity for 14-3-3 and uptake. Addition of a phosphatase to the client protein-loaded coacervates yields in situ dephosphorylation and release of the client protein upon a loss of affinity for 14-3-3-His.

readily partition to the coacervate phase with an excess of positive charge.^[32] Hence, the partitioning of the selected FITC-labeled peptides between the bulk phase and the coacervates was evaluated in the absence and presence of 14-3-3-His, preloaded in coacervates (Figure 1a). This process was first studied in absence of 14-3-3 using confocal microscopy of coacervates in the presence of 100 nM of the peptides (Figure 1b; Figure S4a, Supporting Information). Peptides showed different degrees of partitioning based on their physicochemical properties. As coacervates were prepared with an excess of positively charged Q-Am, positively charged peptides experienced electrostatic repulsion while negatively charged peptides were attracted to the coacervates. This is demonstrated by the exclusion of the ChREBP peptide, which has a +7 net charge, whereas the ER α peptide with a -4 net charge did partition to the coacervate. Other nonspecific interactions also influenced partitioning; the BiExoS peptide (net charge: -4) and the c-Raf pS233/pS259 peptide (net charge: -2) did not partition

effectively and we speculate this to be due to their relatively hydrophobic linkers.

Next, 100 nM of the peptides were added to coacervate samples preloaded with 100 nM of DyLight 650-labeled 14-3-3-His, and the samples were analyzed by confocal microscopy (Figure 1c; Figure S4b, Supporting Information). Peptides that bind to 14-3-3-His with a K_D that is below the local 14-3-3-His concentration were expected to show enhanced partitioning in the presence of 14-3-3-His. Microscopy images were quantified to show the 14-3-3-His-dependent change in mean fluorescence intensity (MFI), normalized to the coacervates with peptide only (Figure 1d; Figure S4c, Supporting Information). Surprisingly, the ChREBP peptide did not show an increase in uptake in the presence of 14-3-3-His, although it should bind with reasonable affinity (K_D : $0.98 \pm 0.06 \mu\text{M}$). Its low uptake might be explained by electrostatic repulsion with the coacervate core. The ER α , Tau, BiExoS, and c-Raf pS233/pS259 peptides showed enhanced

Table 1. Overview of 14-3-3 binding peptides used in this work. Affinities (K_D) were determined by FA assay and presented as mean \pm standard error.

Peptide name	Amino acid sequence	K_D	Charge ^{e)}
TAZ pS89	RSH(pS)SPASLQLGT	$0.043 \pm 0.008 \mu\text{M}^{\text{a}}$	-1
c-Raf pS233/pS259	QHRY(pS)TPHAFTFNTSSPSSEGLSQRQRST(pS)TPNVH	$0.050 \pm 1 \mu\text{M}^{\text{a,b}}$	-2
ChREBP α 2	RDKIRLNNAIWRRAWYIYVKKRRKSPV	$0.98 \pm 0.06 \mu\text{M}$	+7
ER α pT594	AEGFPA(pT)V	$1.2 \pm 0.0 \mu\text{M}$	-4 ^{f)}
BiExoS L423A	QGLADALDLASGGGGGGGGGGQGLADALDLAS	$5.2 \pm 0.2 \mu\text{M}$	-4
Tau pS214	SRTP(pS)LPTPTRE	$\approx 100 \mu\text{M}^{\text{c)}$	-1
c-Raf S233/S259	QHRYSTPHAFTFNTSSPSSEGLSQRQRSTSTPNVH	n.m. ^{d)}	+2

^{a)} Assay limit at a peptide concentration of 100 nM; ^{b)} Two binding events were observed; the second event was excluded from fitting (see Figure S3, Supporting Information); ^{c)} Upper plateau not observed; ^{d)} No binding response observed; ^{e)} Net charge at pH 7; ^{f)} ER α has a free C terminus, the other peptides are C-terminally acetylated.

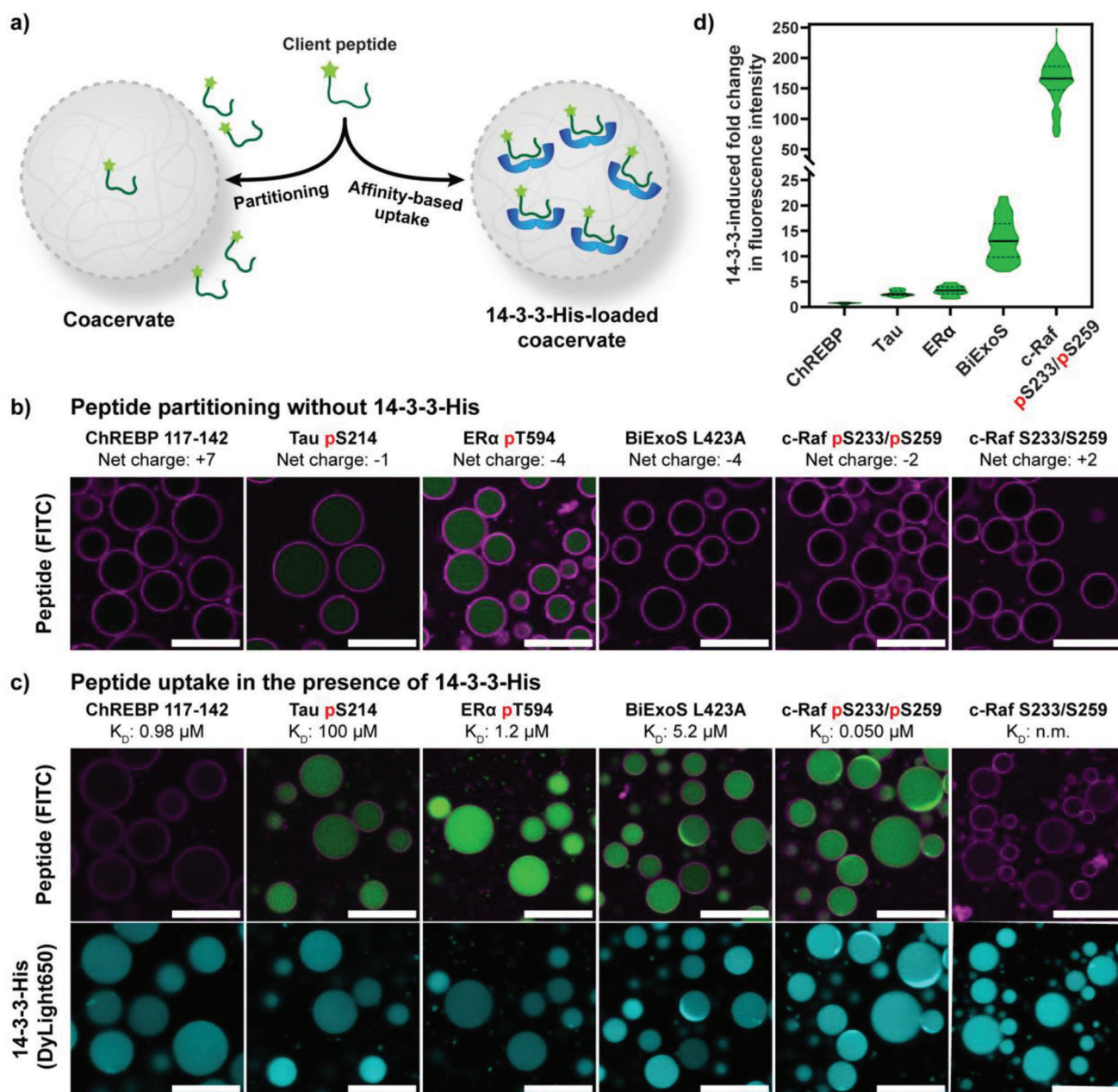


Figure 1. a) Schematic overview of 14-3-3-binding peptide uptake in empty coacervates or 14-3-3-His-loaded coacervates. b) Confocal micrographs displaying the partitioning of different peptides (100 nm) in empty coacervates, shown as an overlay with Nile Red (magenta) as a membrane staining agent. c) Confocal microscopy images displaying the uptake of peptides (100 nm) in 14-3-3-His-loaded (100 nm) coacervates, also shown as an overlay with Nile Red (magenta) in the case of the FITC channel. d) Quantification of the 14-3-3-induced change in mean fluorescence intensity of coacervates, normalized to the fluorescence intensity in coacervates without 14-3-3. The solid lines inside the violin plot represent the median, dashed lines represent the upper and lower quartiles. $N \geq 43$ coacervates. Scale bars: 25 μm . Uncropped images and a zoomed-in version of (d) are available in Figure S4, Supporting Information.

uptake in the presence of 14-3-3-His in comparison to the coacervates that were not 14-3-3-His-loaded. c-Raf pS233/pS259 showed the highest fold-change (161-fold) in uptake induced by the presence of 14-3-3-His. Slight variations in 14-3-3-His-loading were observed between the coacervate samples in Figure 1c, with a maximum difference of 1.8-fold in median 14-3-3-His concentration (Figure S4d, Supporting Information), although these variations do not account for the differences in 14-3-3-His-dependent

uptake of the peptides. The non-phosphorylated c-Raf S233/S259 peptide, a control peptide that does not bind to 14-3-3, did not show enhanced partitioning in the samples with 14-3-3-His (data could not be quantified as fold change). Importantly, the change in net charge (from +2 to -2) due to the two phosphorylated residues of c-Raf pS233/pS259 did not yield a detectable increase in the mean fluorescence intensity, as shown in Figure S5 (Supporting Information). Hence, for the c-Raf

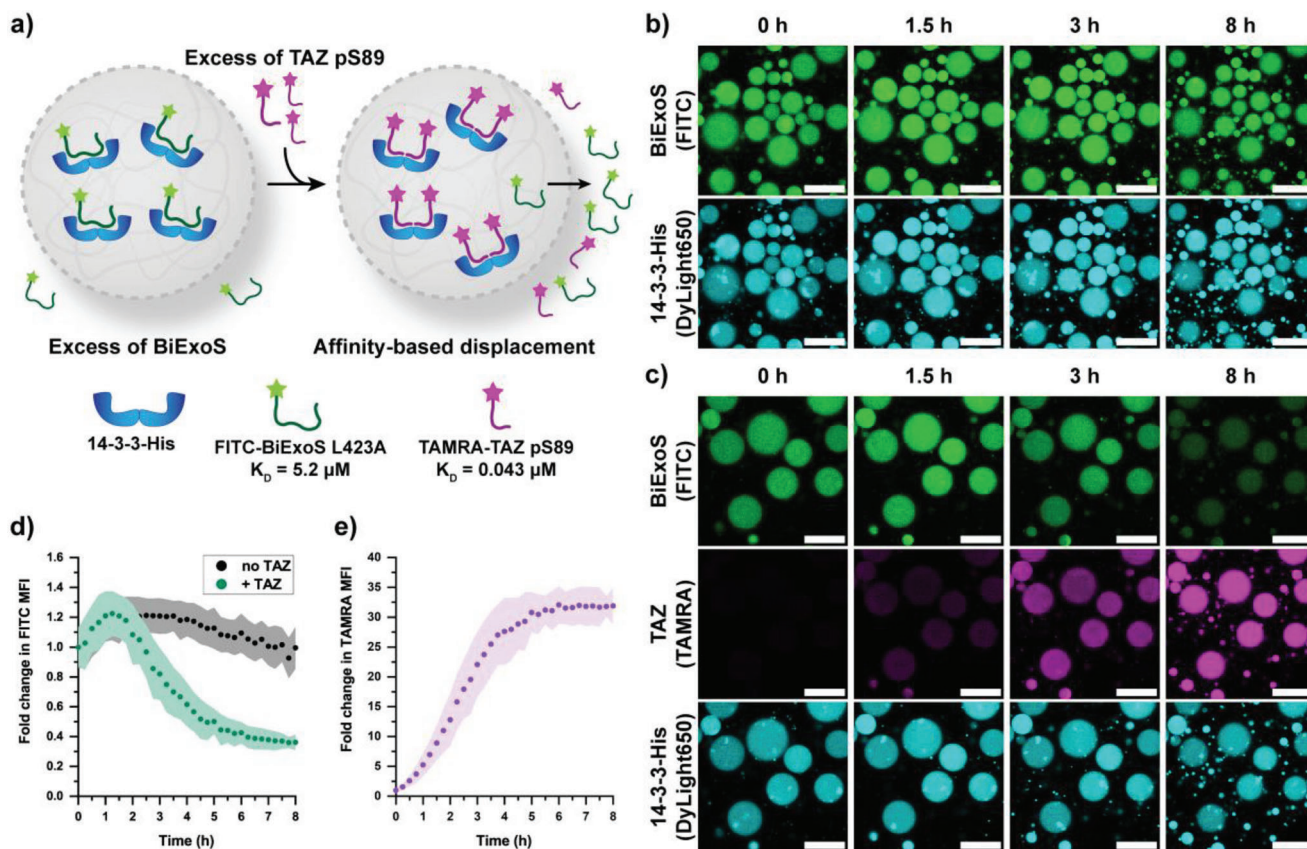


Figure 2. a) Schematic overview of affinity-based displacement experiment. Coacervates are loaded with 14-3-3-His (100 nM) complexed with the FITC-BiExoS peptide (threefold molar excess with respect to 14-3-3 binding sites). Upon addition of the TAMRA-TAZ peptide (1.5-fold molar excess with respect to 14-3-3 binding sites), the TAZ peptide displaces the BiExoS peptide from 14-3-3 due to a 100-fold difference in affinity. b, c) Confocal microscopy images taken over time showing 14-3-3-His/BiExoS-loaded coacervates (b) and 14-3-3-His/BiExoS-loaded coacervates with the TAZ peptide added at $t = 0$ h (c). Scale bar: 25 μm . d, e) Quantification of fluorescence intensity of BiExoS (d) and TAZ (e) in coacervates over time. Data were normalized to the intensity at the initial timepoint and represented as mean \pm standard deviation, $N \geq 31$ coacervates at each timepoint. Uncropped images are available in Figure S9, Supporting Information.

peptide, phosphorylation does not yield detectable charge-based uptake and its uptake is purely 14-3-3-His-dependent.

Furthermore, to analyze the mobility of c-Raf pS233/pS259 bound to 14-3-3-His, a fluorescence recovery after photobleaching (FRAP) experiment was carried out (Figure S6, Supporting Information). Here, c-Raf and 14-3-3 were bleached simultaneously using dual color FRAP, and recovery of fluorescence intensity was analyzed over time and the apparent diffusion constant D_{app} was derived for both samples. It was found that bound c-Raf pS233/pS259 had a D_{app} of $0.043 \pm 0.001 \mu\text{m}^2 \text{s}^{-1}$, whereas 14-3-3-His had a D_{app} of $0.032 \pm 0.000 \mu\text{m}^2 \text{s}^{-1}$, which is in the same order of magnitude. The FRAP experiment was performed with c-Raf pS233/pS259 peptide in a coacervate sample in the absence of 14-3-3-His, where the free peptide was found to have a higher mobility with a D_{app} of $0.209 \pm 0.018 \mu\text{m}^2 \text{s}^{-1}$, although the signal intensity was rather low due to the low partitioning of the peptide. The 14-3-3-dependent change in diffusional mobility was also validated with FRAP of ER α (Figure S7, Supporting Information). The reduced diffusional mobility of peptides in the presence of 14-3-3-His indicates the mobility of peptides to be governed by the mobility of 14-3-3-His, mediated by binding to Ni-NTA-Am.

14-3-3 has a wide range of binding partners with varying affinity, which allows for competition experiments,^[43] in which affinity-based uptake and displacement are carried out using two peptides with different affinities for 14-3-3-His (Figure 2a). Here, coacervates were preloaded with 14-3-3-His and FITC-labeled BiExoS L423A (K_D : $5.2 \pm 0.2 \mu\text{M}$) using an incubation period of 24 h. The BiExoS peptide showed strongly enhanced uptake (13-fold) in the coacervates in the presence of 14-3-3-His. The TAZ pS89 peptide (K_D : $0.043 \pm 0.008 \mu\text{M}$) with tetramethylrhodamine (TAMRA) fluorescent label was selected as the competing peptide, because of its high affinity for 14-3-3-His. The TAZ peptide also showed 14-3-3-His-dependent partitioning (Figure S8, Supporting Information). Both peptides were added at an excess relative to 14-3-3-His binding sites to demonstrate a system where the uptake of peptides is limited by the availability of 14-3-3-His binding sites. TAZ was expected to displace BiExoS from the coacervates over time due to the >100 -fold lower K_D for its interaction with 14-3-3-His. Confocal micrographs were taken over time, allowing for tracking of both peptides independently due to their different fluorescent labels. No significant decrease in fluorescence intensity was observed in coacervates loaded with 14-3-3-His and BiExoS during 8 h when there was no external

addition of TAZ, as analyzed by confocal microscopy (Figure 2b; Figure S9a, Supporting Information). An initial increase in fluorescence intensity can be explained by the sedimentation of several smaller coacervates with higher fluorescence intensity into the focal plane. Upon addition of the TAZ peptide to coacervate samples with 14-3-3-His and BiExoS, a decrease in BiExoS fluorescence intensity and an increase in TAZ fluorescence intensity were observed (Figure 2c; Figure S9b, Supporting Information). Quantification of the micrographs yielded a 64% release of BiExoS, while TAZ was taken up with a 32-fold increase in MFI compared to the initial timepoint (Figure 2d,e). Similar uptake speed was observed when the TAZ peptide was added to coacervates loaded with 14-3-3-His only (Figure S10, Supporting Information); the time to reach equilibrium, therefore, does not seem affected by the presence of BiExoS. Nonetheless, the uptake of TAZ in coacervates with TAZ peptide-only was higher compared to the sample which also contained BiExoS, which can be explained by a remaining amount of the 14-3-3-BiExoS complex. In a control experiment, the BiExoS peptide was added to a coacervate sample with preloaded 14-3-3-TAZ complex, and no displacement of the TAZ peptide was observed over time, as expected (Figure S11, Supporting Information). This demonstrates that the displacement of BiExoS by TAZ is indeed based on a difference in affinity for 14-3-3-His, rather than on the order of addition of the peptides.

The displacement of BiExoS by TAZ demonstrates that the uptake of 14-3-3 binding partners is both dynamic and thermodynamically controlled for 14-3-3-His. These results are in good agreement with the intrinsic affinity measured in conventional protein titration assays. Since BiExoS can bind in a bivalent manner, thereby occupying both binding sites of a 14-3-3 dimer, BiExoS, and TAZ are not expected to be able to bind to the same 14-3-3 dimer. However, since the FITC-labeled BiExoS peptide could undergo Förster resonance energy transfer (FRET) with the TAMRA-labeled TAZ peptide upon excitation of FITC, the samples were analyzed by fluorescence spectroscopy after the displacement experiment (Figure S12, Supporting Information). Gratifyingly, no signal for TAMRA was observed upon excitation of BiExoS.

To offer additional insight into the displacement experiment, it was simulated using a thermodynamic equilibrium model (Figure S13, Supporting Information). The estimated local concentrations of 14-3-3-His (64 μM) and BiExoS (64 μM of binding sites) and the K_D values determined from FA assays were given as input, and the presence of each species was determined at varying [TAZ]. It was calculated that 14-3-3-His should be occupied by 88% with TAZ when the TAZ concentration is at 64 μM , with 10% of 14-3-3-His still bound to BiExoS. This supports the experimental findings of TAZ-mediated displacement with a minor fraction of 14-3-3 still occupied with BiExoS. The slightly higher retention of BiExoS observed experimentally than predicted by the model may be due to a difference in net charge between the BiExoS (-4) and the TAZ (-1) peptides.

2.2. Phosphorylation-Regulated Protein Recruitment

After establishing affinity-based uptake of peptide derivatives of 14-3-3 binding partners, we sought to analyze full-length pro-

tein recruitment. Green fluorescent protein (GFP) was selected as a model protein as it was previously shown that it is mostly excluded in this coacervate system, unless uptake was mediated by a His-tag.^[32] The c-Raf-S233/S259 binding domain was fused to GFP, forming the 35 kDa GFP-c-Raf S233/S259 (GFP-c-Raf) non-His-tagged fusion protein. The c-Raf peptide domain was selected for its phosphorylation- and 14-3-3-dependent uptake (Figure 1b,c). Protein kinase A (PKA, hereafter used to refer to the catalytic subunit of PKA) is known to phosphorylate the S233 and S259 sites in c-Raf.^[47] Hence, it was used for in situ phosphorylation of GFP-c-Raf S233/S259, leading to uptake in coacervates upon external enzymatic regulation (Figure 3a).

Phosphorylation of GFP-c-Raf by PKA in bulk was investigated by liquid chromatography quadrupole time of flight mass spectrometry (LC-MS Q-ToF). Signals corresponding to GFP-c-Raf S233/S259 with two and three phosphorylated residues were found (Figures S14–S16, Supporting Information). Two of these phosphorylation sites were located on the c-Raf S233/S259 domain, presumably on S233 and S259. Since the c-Raf S233/S259 domain was presumably correctly doubly phosphorylated, it was assumed that binding to 14-3-3-His would not be impaired for the triply phosphorylated species. Indeed, strong phosphorylation- and 14-3-3-His-dependent uptake was confirmed for GFP-c-Raf, as analyzed by confocal microscopy (Figure S17, Supporting Information).

Next, PKA (non-His-tagged) was used for in situ external phosphorylation, uptake, and binding of GFP-c-Raf. In coacervates with 100 nm of 14-3-3-His, 100 nm GFP-c-Raf S233/S259, and PKA, omitting phosphorylation agent ATP yielded no increase in GFP-c-Raf fluorescence intensity over time, as analyzed by confocal microscopy (Figure 3b). Phosphorylation-mediated uptake was observed via an increase in GFP-c-Raf fluorescence intensity in the presence of ATP (Figure 3c). Phosphorylation by PKA was found to yield a 72-fold enhanced uptake of GFP-c-Raf (Figure 3d), after quantification of MFI at each time point. This demonstrates that external stimuli can be applied to regulate the protein composition of coacervates.

The timescale of PKA-mediated uptake of GFP-c-Raf was compared with PKA-mediated uptake of the FITC-labeled peptide (Figure S18, Supporting Information). It was found that FITC-c-Raf was taken up more rapidly, with equilibrium reached after approximately six hours, indicating that diffusion might be a limiting factor for PKA-mediated uptake of GFP-c-Raf. To assess the importance of diffusion, pre-phosphorylated FITC-c-Raf, and GFP-c-Raf were added to 14-3-3-loaded coacervates, and their uptake was analyzed (Figure S19, Supporting Information). The peptide was taken up within three hours, whereas GFP-c-Raf took more than eight hours, which is likely an effect of size of the clients, as GFP-c-Raf is more favorably charged (net charge: -9 for the phosphorylated protein) for uptake in the positively charged coacervates than the FITC peptide (net charge: -2). This demonstrates that indeed diffusion into coacervates requires more time for the GFP fusion protein, contributing to its relatively slow PKA-mediated uptake. Next, GFP-c-Raf pS233/pS259 loaded in coacervates with 14-3-3-His was bleached in a FRAP experiment to analyze its diffusivity. This yielded a D_{app} of $0.041 \pm 0.001 \mu\text{m}^2 \text{s}^{-1}$ (Figure S20, Supporting Information), which is in good agreement with the D_{app} values for 14-3-3-His and 14-3-3-His-bound FITC-c-Raf pS233/pS259. This

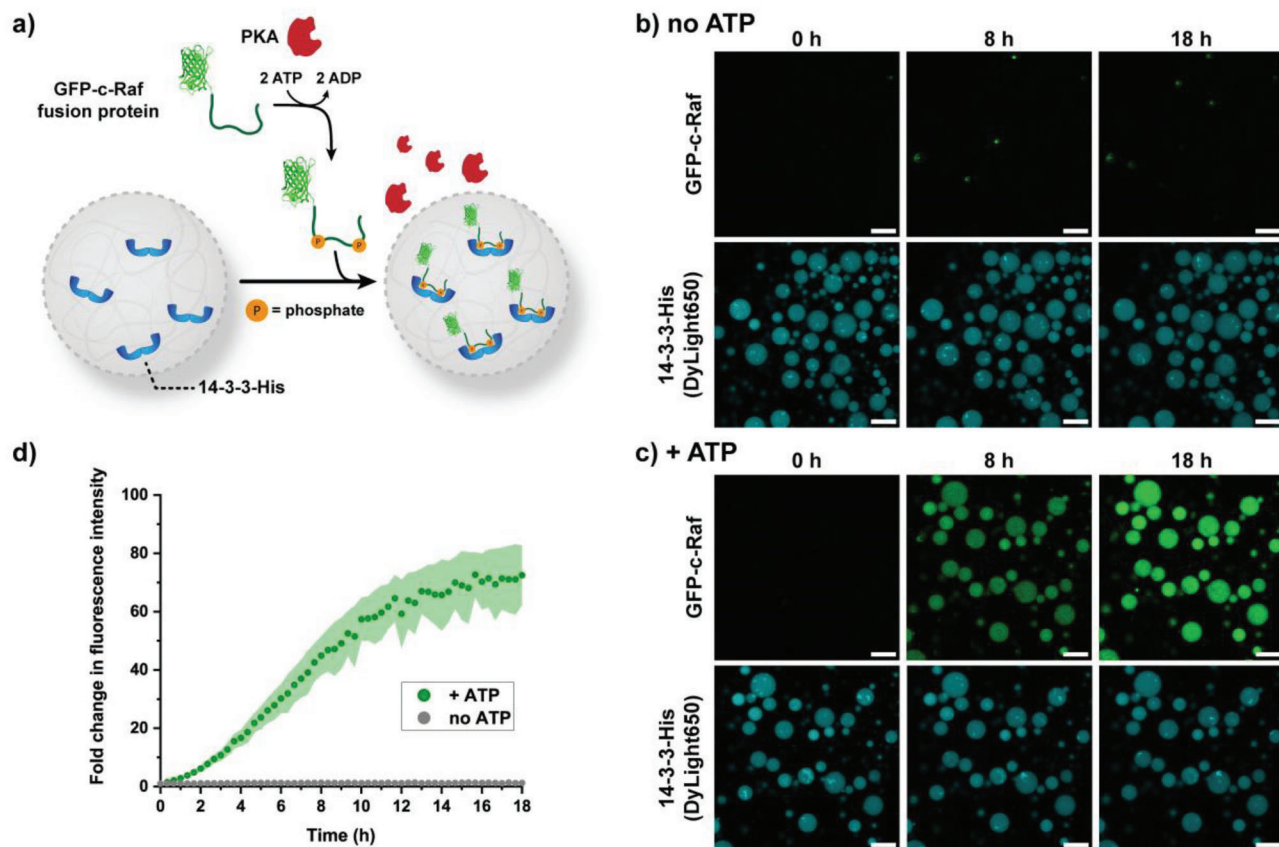


Figure 3. Kinase-regulated uptake of GFP-c-Raf. a) Schematic overview of in situ phosphorylation of GFP-c-Raf S233/S259 by non-His-tagged (external) PKA, leading to uptake of GFP-c-Raf in coacervates based on affinity for 14-3-3-His. b,c) Confocal microscopy images over time showing fluorescence intensity of GFP-c-Raf and 14-3-3-His in samples with PKA in the absence of ATP (b) and in the presence of ATP (c). GFP-c-Raf (100 nM) was added to coacervates with 14-3-3-His (100 nM), PKA (15 U μL^{-1}). In the case of (c), ATP (100 μM) was added directly before microscopy. Scale bar: 25 μm . d) Quantification of fluorescence intensity of GFP-c-Raf over time of experiment (b) and (c). Data were normalized to the intensity at the initial timepoint and represented as mean \pm standard deviation, $N \geq 31$ coacervates at each timepoint.

demonstrates that the internal diffusional mobility of the GFP-fusion protein, much like the FITC-peptide, was mostly governed by the mobility of 14-3-3-His, and not by the size of the client species.

Recruitment of client proteins to biomolecular condensates is typically reversible to allow for both activation and deactivation of certain signaling pathways or processes.^[6] We envisioned that phosphatase activity would be able to reverse client protein binding, since binding is in our case based on phosphorylation state. We, therefore, used a His-tagged construct of the catalytic domain of protein phosphatase 1 α (PP1c-His), a Mn^{2+} -dependent serine/threonine phosphatase, for in-situ dephosphorylation of the c-Raf pS233/pS259 domain (Figure 4a). PP1c-His was expressed in good purity, and its activity was analyzed by FA assay in bulk, showing dephosphorylation of the c-Raf pS233/pS259 peptide (Figures S21 and S22, Supporting Information). It should be noted that in the FA assay, relatively high concentrations of phosphatase were used and full dephosphorylation was not achieved. Since the c-Raf domain binds to 14-3-3 with a high affinity, it is hypothesized that dephosphorylation was limited by the dissociation of the 14-3-3-c-Raf pS233/pS259 complex, which has been suggested as a general regulatory mechanism of 14-3-3 for its phosphorylated client proteins.^[48,49]

Next, the activity of PP1c-His inside coacervates was analyzed over time by confocal microscopy. In coacervates loaded with the complex of 14-3-3-His (100 nM) and GFP-c-Raf pS233/pS259 (100 nM), relatively constant fluorescence was observed over time (Figure 4b). Upon the addition of PP1c-His (10 nM) directly before microscopy, a decrease in fluorescence intensity was observed (Figure 4c). This PP1c-His-mediated release of GFP-c-Raf was quantified (Figure 4d) and found to yield a 29% release of GFP-c-Raf at the 16 h timepoint. Full dephosphorylation was not observed, which is in agreement with the results found in the bulk FA assay. This system demonstrates the reversibility of phospho-regulated uptake of client proteins. In a control experiment, the release of FITC-c-Raf pS233/pS259 peptide from 14-3-3-His loaded coacervates by PP1c-His was analyzed over time (Figure S23, Supporting Information). The fact that both peptide and protein were released with similar rates indicated that the limiting step is dephosphorylation rather than diffusion.

2.3. Phosphorylation-Regulated Binding of Preloaded Proteins

After demonstrating reversible, affinity-based recruitment of client proteins to the 14-3-3-scaffold protein in artificial cells, we

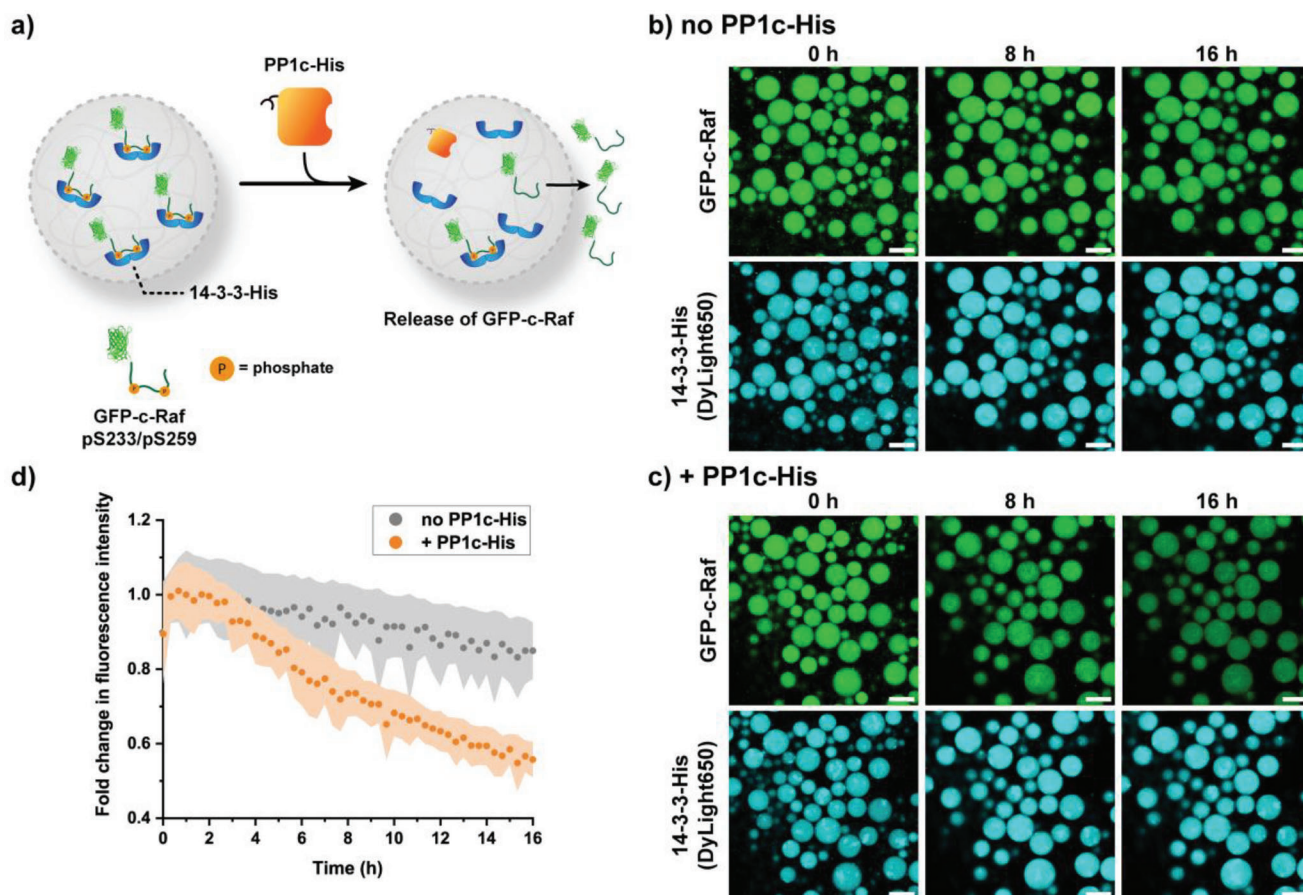


Figure 4. Phosphatase-regulated release of GFP-c-Raf from coacervates loaded with the phosphorylated GFP-c-Raf-14-3-3 complex. a) Schematic overview of complex dissociation by in situ dephosphorylation of GFP-c-Raf pS233/pS259 after the introduction of PP1c-His, leading to the release of GFP-c-Raf upon loss of affinity for 14-3-3-His. b,c) Confocal microscopy images over time showing fluorescence intensity of GFP-c-Raf (100 nm) and 14-3-3-His (100 nm) in the absence of PP1c-His (b) and in the presence of PP1c-His (10 nM) (c). PP1c-His was added directly before microscopy. Scale bars: 25 μm . d) Quantification of fluorescence intensity of GFP-c-Raf over time of the experiments (b) and (c). Data were normalized to the intensity at the 1 h timepoint because of the settling of coacervates in the first hour. The data are represented as mean \pm standard deviation, $N \geq 93$ coacervates at each timepoint.

sought to investigate if 14-3-3 could also be used as a docking station to bring together two proteins that were already localized in the coacervate for the reconstitution of function. Hence, a protein complementation assay using the split NanoLuc luciferase was used, which generates bioluminescence upon complementation of two fusion proteins and conversion of its substrate furimazine.^[50] The split luciferase consisted of an 18 kDa fragment, LgBiT, which was fused to the c-Raf S233/S259 domain (LgBiT-c-Raf S233/S259-His, LgBiT-c-Raf-His in short) to facilitate protein expression and to mimic a full length protein. The second part of the luciferase, a 1 kDa fragment named SmBiT, was fused to a 14-3-3 dimer, yielding dT14-3-3-SmBiT-His. Here, a recombinantly linked dimer of 14-3-3 was used to promote 1:1 split NanoLuc complex formation with bivalent LgBiT-c-Raf-His. Several variants of the SmBiT have been reported with a range of affinities for LgBiT. The lowest affinity SmBiT/LgBiT pair was chosen ($K_D = 190 \mu\text{M}$)^[50] to prevent background complementation induced by affinity between LgBiT and SmBiT rather than affinity between 14-3-3 and the c-Raf domain. LgBiT-c-Raf

S233/S259-His binds to dT14-3-3-SmBiT-His upon phosphorylation by PKA, promoting reconstitution of the split NanoLuc by an increased local concentration of LgBiT and SmBiT (Figure 5a). To allow phosphorylation inside the coacervates, a His-tagged construct of PKA was designed, which was expressed in good purity and found to rapidly phosphorylate FITC-c-Raf S233/S259 in an FA assay (Figures S24 and S25, Supporting Information).

The split NanoLuc assay was evaluated in coacervates using bioluminescence spectroscopy (Figure 5b). dT14-3-3-SmBiT-His (250 nm), LgBiT-c-Raf S233/S259-His (250 nm), and PKA-His (25 nm) were loaded in the coacervates in the presence of ATP and furimazine. Bioluminescence was enhanced sevenfold in the PKA-His-containing sample compared to the control sample without PKA-His. The reaction rate of split-NanoLuc inside the coacervates was limited by partitioning of the substrate; bioluminescence spectroscopy over time revealed a relatively constant signal in coacervates (Figure S26, Supporting Information). In bulk solution, a higher initial bioluminescence signal was found, with rapid decay of the signal over time.

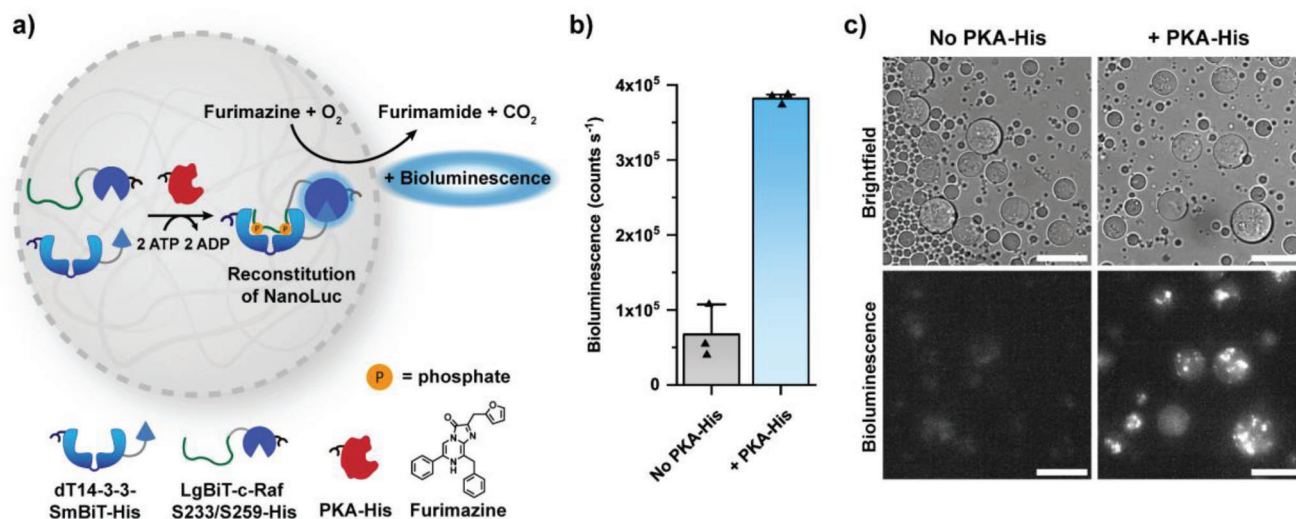


Figure 5. Split-NanoLuc complementation assay for preloaded interaction partners. a) Schematic overview of coacervates loaded with dT14-3-3-SmBiT-His, LgBiT-c-Raf S233/S259-His, and PKA-His. Binding between the 14-3-3 and c-Raf domains upon phosphorylation by PKA-His yields complementation of the split NanoLuc and restores enzymatic activity. Upon the conversion of its substrate furimazine, split NanoLuc generates bioluminescence. b) Bioluminescence spectroscopy of coacervate samples with dT14-3-3-SmBiT-His (250 nm), LgBiT-c-Raf S233/S259-His (250 nm), and ATP (100 μM), in the absence or presence of PKA-His. Samples were incubated overnight before furimazine was added (1:240 dilution) and the measurement was started, with bioluminescence analyzed at 458 ± 12.5 nm. N = 3. c) Bioluminescence microscopy of samples with the same conditions as (b), with bright-field images as reference (top), and images taken using a DAPI filter without excitation (bottom). Scale bar: 25 μm. Uncropped images are provided in Figure S28, Supporting Information.

Confocal microscopy and bioluminescence microscopy were used to verify that functional reconstitution of luciferase actually occurred within the artificial cells. With the former technique, it was demonstrated that dT14-3-3-SmBiT-His was taken up in the coacervates (Figure S27, Supporting Information). With the latter, a clear bioluminescence signal was observed from inside the coacervates (Figure 5c; Figures S28 and S29, Supporting Information), when evaluated alongside the bright-field images. In accordance with spectroscopy, the sample with PKA-His showed an enhanced bioluminescence signal in the micrographs when compared to the control sample without PKA-His. The heterogeneous distribution of bioluminescence is likely caused by protein aggregation, which might be explained by the relatively high local concentration of proteins and the strong multivalent interactions mediated by 14-3-3. The protein cargo within those aggregates still yields a bioluminescence signal and is therefore thought to be functional despite aggregation.

With the split NanoLuc system we demonstrate that 14-3-3-loaded artificial cells are not only capable of reversible, enzyme-mediated recruitment of client proteins externally, but also internally, which is even more relevant from a biological perspective. The dependence of substrate localization on phosphorylation is reminiscent of PKA regulation, where substrate tethering, independent of the active site, is used to modulate activity or specificity.^[51,52] Likewise, PKA activity can also be regulated by recruitment to condensates.^[15] By showing modulation of kinase activity and specificity by recruitment of the enzyme and/or the substrate to condensates. Hence, our system represents an attractive model to study the principles of natural regulation of kinase activity in condensates.

3. Conclusion

A coacervate-based artificial cell platform based on amylose-derived polyelectrolytes was applied to reconstitute native interactions between client peptides and proteins and the 14-3-3 scaffold protein. The interactions of clients and 14-3-3 were dependent on the client's phosphorylation state, which can be enzymatically regulated using phosphorylation and dephosphorylation processes. 14-3-3-His was efficiently immobilized in the coacervates, and it was shown that peptide cargo can be recruited to the coacervates based on its affinity for 14-3-3. Furthermore, a displacement experiment was used to demonstrate competitive binding between two peptides governed by their different affinity for 14-3-3. Besides peptides, proteins could be reversibly recruited by in situ phosphorylation using a kinase. Similarly, the addition of a phosphatase to coacervates led to release of the client protein upon dephosphorylation. Besides uptake and release of client proteins into or from the artificial cell platform, also intracellular organization was induced. For this purpose a split-luciferase assay was used; the two parts of the enzyme were preloaded in the coacervate but functionally tethered upon phosphorylation and binding to 14-3-3. This demonstrates that kinase activity and specificity can be regulated by changes in localization of the enzyme and substrate. This work serves as a model system for studying native PPIs, with fundamental potential to study biophysical phenomena such as regulated client recruitment to LLPS droplets.

In future work, the mechanisms shown here could be applied to study dynamically regulated scaffold protein interactions. This could for example be used in a synthetic signaling context, where communication between distinct populations of coacervates is

regulated by PPIs. Applying enzymatically controlled native PPIs for such synthetic signaling systems could offer insight into the biophysical phenomena of chemical signaling.

Supporting Information

Supporting Information is available from the Wiley Online Library or from the author.

Acknowledgements

The Dutch Ministry of Education, Culture, and Science (Gravitation Program 024.001.035) is acknowledged for funding. Joost van Dongen and Sebastiaan van den Wildenberg are thanked for Q-ToF LC-MS measurements. Dr. Mark van Turnhout and Dr. Yuyang Wang are thanked for assisting with bioluminescence microscopy. Dr. Peter Cossar and Bente Somsen are thanked for fruitful discussions regarding the peptide displacement experiment.

Note: The cited figure in the sentence "The c-Raf peptide domain was selected for its phosphorylation- and 14-3-3-dependent uptake (Figure 1b,c)", in the first paragraph of Section 2.2 "Phosphorylation-Regulated Protein Recruitment" was corrected from Figure 2b,c on July 20, 2023, after initial publication online.

Conflict of Interest

The authors declare no conflict of interest.

Author Contributions

T.W.V., W.J.A., and L.J.M.L. designed the experiments and analyzed the experimental results. W.J.A. and L.J.M.L. performed initial experiments. T.W.V. and M.A.M.V. performed the experiments in this work. L.B. and J.C.M.H. conceived and supervised the project. A.F.M. and M.M. provided feedback on the results. T.W.V. wrote the manuscript with the aid and input of all other authors.

Data Availability Statement

The data that support the findings of this study are available from the corresponding author upon reasonable request.

Keywords

artificial cells, coacervates, phosphorylation, scaffold proteins, synthetic signaling

Received: January 31, 2023
Revised: March 20, 2023
Published online: May 31, 2023

- [1] M. C. Good, J. G. Zalatan, W. A. Lim, *Science* **2011**, 332, 680.
- [2] M. Beck, M. Topf, Z. Frazier, H. Tjong, M. Xu, S. Zhang, F. Alber, *J Struct Biol* **2011**, 173, 483.
- [3] C. Q. Pan, M. Sudol, M. Sheetz, B. C. Low, *Cell Signal* **2012**, 24, 2143.
- [4] D. Garbett, A. Bretscher, *Mol. Biol. Cell* **2014**, 25, 2315.

- [5] S. F. Banani, A. M. Rice, W. B. Peeples, Y. Lin, S. Jain, R. Parker, M. K. Rosen, *Cell* **2016**, 166, 651.
- [6] J. A. Ditlev, L. B. Case, M. K. Rosen, *J. Mol. Biol.* **2018**, 430, 4666.
- [7] C. P. Brangwynne, C. R. Eckmann, D. S. Courson, A. Rybarska, C. Hoegel, J. Gharakhani, F. Jülicher, A. A. Hyman, *Science* **2009**, 324, 1729.
- [8] T. Mittag, R. V. Pappu, *Mol. Cell* **2022**, 82, 2201.
- [9] Y. Shin, C. P. Brangwynne, *Science* **2017**, 357, 1253.
- [10] S. F. Banani, H. O. Lee, A. A. Hyman, M. K. Rosen, *Nat. Rev. Mol. Cell Biol.* **2017**, 18, 285.
- [11] Q. Su, S. Mehta, J. Zhang, *Mol. Cell* **2021**, 81, 4137.
- [12] T. Mittag, R. Parker, *J. Mol. Biol.* **2018**, 430, 4636.
- [13] J. R. Espinosa, J. A. Joseph, I. Sanchez-Burgos, A. Garaizar, D. Frenkel, R. Collepardo-Guevara, *Proc. Natl. Acad. Sci. USA* **2020**, 117, 13238.
- [14] S. Sridharan, A. Hernandez-Armendariz, N. Kurzawa, C. M. Potel, D. Memon, P. Beltrao, M. Bantscheff, W. Huber, S. Cuylen-Haering, M. M. Savitski, *Nat. Chem. Biol.* **2022**, 18, 1104.
- [15] D. Sang, T. Shu, C. F. Pantoja, A. Ibáñez de Opakua, M. Zweckstetter, L. J. Holt, *Mol. Cell* **2022**, 82, 3693.
- [16] S. Markmiller, S. Soltanieh, K. L. Server, R. Mak, W. Jin, M. Y. Fang, E. C. Luo, F. Krach, D. Yang, A. Sen, A. Fulzele, J. M. Wozniak, D. J. Gonzalez, M. W. Kankel, F. B. Gao, E. J. Bennett, E. Lécuyer, G. W. Yeo, *Cell* **2018**, 172, 590.
- [17] S. Jain, J. R. Wheeler, R. W. Walters, A. Agrawal, A. Barsic, R. Parker, *Cell* **2016**, 164, 487.
- [18] T. P. López-Palacios, J. L. Andersen, *Trends Cell Biol.* **2022**, <https://doi.org/10.1016/j.tcb.2022.11.009>.
- [19] W. P. Lipiński, B. S. Visser, I. Robu, M. A. A. Fakhree, S. Lindhoud, M. M. A. E. Claessens, E. Spruijt, *Sci. Adv.* **2022**, 8, eabq6495.
- [20] N. A. Yewdall, A. F. Mason, J. C. M. Van Hest, *Interface Focus* **2018**, 8, 20180023.
- [21] N. A. Yewdall, A. A. M. André, T. Lu, E. Spruijt, *Curr. Opin. Colloid Interface Sci.* **2021**, 52, 101416.
- [22] M. Guan, M. V. Garabedian, M. Leutenegger, B. S. Schuster, M. C. Good, D. A. Hammer, *Biochemistry* **2021**, 60, 3137.
- [23] B. S. Schuster, E. H. Reed, R. Parthasarathy, C. N. Jahnke, R. M. Caldwell, J. G. Bermudez, H. Ramage, M. C. Good, D. A. Hammer, *Nat. Commun.* **2018**, 9, 2985.
- [24] M. V. Garabedian, Z. Su, J. Dabdoub, M. Tong, A. Deiters, D. A. Hammer, M. C. Good, *Biochemistry* **2022**, 61, 2470.
- [25] W. Peeples, M. K. Rosen, *Nat. Chem. Biol.* **2021**, 17, 693.
- [26] M. V. Garabedian, W. Wang, J. B. Dabdoub, M. Tong, R. M. Caldwell, W. Benman, B. S. Schuster, A. Deiters, M. C. Good, *Nat. Chem. Biol.* **2021**, 17, 998.
- [27] M. Yoshikawa, T. Yoshii, M. Ikuta, S. Tsukiji, *J. Am. Chem. Soc.* **2021**, 143, 6434.
- [28] E. M. Zhao, N. Suek, M. Z. Wilson, E. Dine, N. L. Pannucci, Z. Gitai, J. L. Avalos, J. E. Toettcher, *Nat. Chem. Biol.* **2019**, 15, 589.
- [29] K. Hong, D. Song, Y. Jung, *Nat. Commun.* **2020**, 11, 5554.
- [30] A. F. Mason, B. C. Buddingh', D. S. Williams, J. C. M. van Hest, *J. Am. Chem. Soc.* **2017**, 139, 17309.
- [31] N. A. Yewdall, B. C. Buddingh', W. J. Altenburg, S. B. P. E. Timmermans, D. F. M. Vervoort, L. K. E. A. Abdelmohsen, A. F. Mason, J. C. M. van Hest, *ChemBioChem* **2019**, 20, 2643.
- [32] W. J. Altenburg, N. A. Yewdall, D. F. M. Vervoort, M. H. M. E. van Stevendaal, A. F. Mason, J. C. M. van Hest, *Nat. Commun.* **2020**, 11, 6282.
- [33] M. H. M. E. van Stevendaal, L. Vasiukas, N. A. Yewdall, A. F. Mason, J. C. M. van Hest, *ACS Appl. Mater. Interfaces* **2021**, 13, 7879.
- [34] C. Ottmann, *Bioorganic Med. Chem.* **2013**, 21, 4058.
- [35] M. Molzan, B. Schumacher, C. Ottmann, A. Baljuls, L. Polzien, M. Weyand, P. Thiel, R. Rose, M. Rose, P. Kuhenne, M. Kaiser, U. R. Rapp, J. Kuhlmann, C. Ottmann, *Mol. Cell. Biol.* **2010**, 30, 4698.
- [36] E. Freed, M. Symons, S. G. Macdonald, F. McCormick, R. Ruggieri, *Science* **1994**, 265, 1713.

- [37] S. Rajagopalan, R. S. Sade, F. M. Townsley, A. R. Fersht, *Nucleic Acids Res.* **2009**, *38*, 893.
- [38] B. Schumacher, J. Mondry, P. Thiel, M. Weyand, C. Ottmann, *FEBS Lett.* **2010**, *584*, 1443.
- [39] C. Johnson, M. Tinti, N. T. Wood, D. G. Campbell, R. Toth, F. Dubois, K. M. Geraghty, B. H. C. Wong, L. J. Brown, J. Tyler, A. Gernez, S. Chen, S. Synowsky, C. MacKintosh, *Mol. Cell. Proteomics* **2011**, *10*, 005751.
- [40] C. Ottmann, L. Yasmin, M. Weyand, J. L. Veessenmeyer, M. H. Diaz, R. H. Palmer, M. S. Francis, A. R. Hauser, A. Wittinghofer, B. Hallberg, *EMBO J.* **2007**, *26*, 902.
- [41] M. Skwarczynska, M. Molzan, C. Ottmann, *Proc. Natl. Acad. Sci. USA* **2013**, *110*, 377.
- [42] S. J. A. Aper, A. Den Hamer, S. F. A. Wouters, L. J. M. Lemmens, C. Ottmann, L. Brunsveld, M. Merck, *ACS Synth. Biol.* **2018**, *7*, 2216.
- [43] A. Hazegh Nikroo, L. J. M. Lemmens, T. Wezeman, C. Ottmann, M. Merck, L. Brunsveld, *ACS Synth. Biol.* **2022**, *11*, 2464.
- [44] C. Johnson, S. Crowther, M. J. Stafford, D. G. Campbell, R. Toth, C. MacKintosh, *Biochem. J.* **2010**, *427*, 69.
- [45] Q. Ge, N. Huang, R. M. Wynn, Y. Li, X. Du, B. Miller, H. Zhang, K. Uyeda, *J. Biol. Chem.* **2012**, *287*, 41914.
- [46] M. L. Henriksson, M. S. Francis, A. Peden, M. Aili, K. Stefansson, R. Palmer, A. Aitken, B. Hallberg, *Eur. J. Biochem.* **2002**, *269*, 4921.
- [47] N. Dumaz, Y. Light, R. Marais, *Mol. Cell. Biol.* **2002**, *22*, 3717.
- [48] L. Sun, G. Stoecklin, S. Van Way, V. Hinkovska-Galcheva, R. F. Guo, P. Anderson, T. P. Shanley, *J. Biol. Chem.* **2007**, *282*, 3766.
- [49] A. Hausser, G. Link, M. Hoene, C. Russo, O. Selchow, K. Pfizenmaier, *J. Cell Sci.* **2006**, *119*, 3613.
- [50] A. S. Dixon, M. K. Schwinn, M. P. Hall, K. Zimmerman, P. Otto, T. H. Lubben, B. L. Butler, B. F. Binkowski, T. Machleidt, T. A. Kirkland, M. G. Wood, C. T. Eggers, L. P. Encell, K. V. Wood, *ACS Chem. Biol.* **2016**, *11*, 400.
- [51] M. Dyla, N. S. González Foutel, D. E. Otzen, M. Kjaergaard, *Proc. Natl. Acad. Sci. USA* **2022**, *119*, e2203098119.
- [52] C. J. Miller, B. E. Turk, *Trends Biochem. Sci.* **2018**, *43*, 380.